Effect of structure parameters of catalyst substrate on the performance of diesel particulate filter

Piqiang Tan*, *Yunpeng* Li, *Chenyang* Cao, *Diming* Lou, and *Zhiyuan* Hu

School of Automobile, Tongji University, Shanghai 201804, PR China

Abstract. The filtration efficiencies of the particulate matter and the particulate number in DPF, the no-load pressure drop of DPF, and the load pressure drop of DPF were selected as key performance parameters of DPF. The influence of the cell density and the wall thickness of the DPF on these key performance parameters of DPF was studied in detail. Firstly, a calculation model of DPF was established, and the compensation mathematical model was added. Secondly, the key performance parameters of DPF were defined. Finally, based on the model, the key performance parameters are numerically investigated under different cell density and wall thickness of the DPF. Consequently, with the increase of cell density of DPF, the filtration efficiency of DPF increases, the load pressure drop of DPF decreases, but the no-load pressure drop of DPF increases. With the decrease of the wall thickness of the DPF, the no-load pressure drop of the DPF decreases, the load pressure drop of the DPF decreases, but the filtration efficiency of the DPF decreases. The most suitable combination scheme is a cell density of 200-300 CPSI and a wall thickness of 11-16 mil.

Keywords: Diesel particulate filter, Filtration efficiency, Pressure drop, Cell density, Wall thickness.

1 Introduction

Due to their high efficiency and stability, good fuel economy and high output power [1], diesel engines are often used as power devices for agricultural machinery. However, due to diesel engines have the characteristics of high particulate matter emissions[2,3], diesel particulate filter (DPF) must be installed to meet stringent emission regulations. The cell density and wall thickness of DPF substrate are key structural parameters that affect the DPF collection efficiency, DPF pressure drop performance and durability. Therefore, when designing DPF, these structural parameters should be considered.

Many researchers have carried out simulations and experimental studies to explore the influence of DPF structural parameters on the performance of DPF, so as to rationally optimize and design the structural parameters of DPF. Zhang et al.[4] evaluated the influence of four structural parameters (the wall thickness, the mean pore diameter, the porosity and

*Corresponding author: tpq2000@163.com

the channel width) on the deterioration of DPF's performance. The results showed that the wall thickness and the channel width are important structural parameters that caused the blockage of the DPF's channel and the thermal aging of the DPF. The University of Thessaly, Greece, Pontikakis et al.[5] built a three-dimensional model for the CDPF as a simulation basis for designing the structure parameters of the filter. Williams [6] of Loughborough University in the United Kingdom established a mathematical model for the influence of the non-uniform distribution of carbon loading in the DPF on the back pressure of the DPF, which can be better combined with the experimental data to analyze and optimize the design of the structural parameters of the DPF. For the non-road diesel engines, Cordiner et al.[7] developed an exhaust aftertreatment system design tool based on GT-Power simulation software combined with a custom mathematical model. Corresponding simulation results can be obtained by inputting relevant design parameters and selecting calculation model. Subsequently, the design plan could be analyzed and changed. Deng et al.[8] studied the influence of key structural parameters on the DPF behavior in equilibrium, and the results indicated that a smaller diameter of DPF substrate may result in a larger pressure drop. Campolo et al.[9] of the University of Udine in Italy established a semi-analytical model to analyze the characteristics of DPF in the trap and regeneration stages. Based on this model, the influences of channel number, size, permeability, heat capacity of filter on the DPF back pressure, filtration efficiency and regeneration efficiency were explored, and the results were used as the basis to optimize the design of DPF structural parameters.

In summary, the research on the influence of structural parameters of DPF substrate on DPF performance was relatively scattered. The most important structural parameters such as cell density and wall thickness of DPF were selected in this paper, and the corresponding numerical simulation research was carried out. This work will provide certain guiding significance for the structural design of DPF substrate.

2 Modeling

2.1 DPF simulation compensation mathematical model

Due to AVL-Boost lacks a built-in model for the calculation of some key parameters in the process of wall-flow DPF trapping and flowing, which seriously affects the simulation results. A compensation mathematical model of some key parameters was established and embedded into the DPF simulation model.

2.1.1 DPF classic filtration theory

The trapping of particles by wall-flow DPF is divided into two stages: the deep-bed filtration and the cake filtration[10], as shown in Figure 1. When the blank filter starts to trap, the trapped soot particles firstly deposit into the filter wall, which is the deep-bed filtration phase. With the accumulation of soot particles, the porosity and pore size of the filter will decrease. When it decreases to a certain value, the carbon load inside the filter wall reaches saturation, and the deep-bed filtration phase ends. Subsequently, the trapped soot particles will be deposited on the filter wall to form a cake layer, which means entering the cake filtration phase.

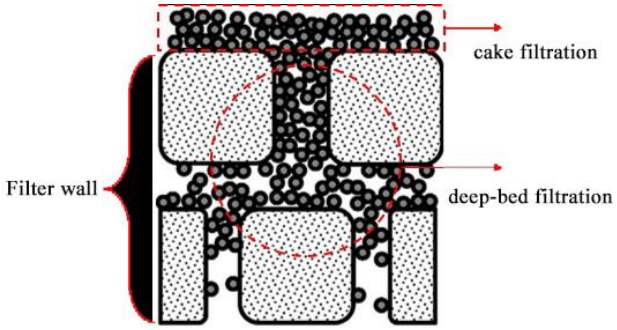

Fig. 1. Schematic diagram of DPF filtration phase.

At present, in the field of simulation modeling of the wall-flow DPF filtration process, most models are based on the "unit collector" assumption when calculating the carbon load of the deep-bed filtration phase [10-12], as shown in Figure 2.

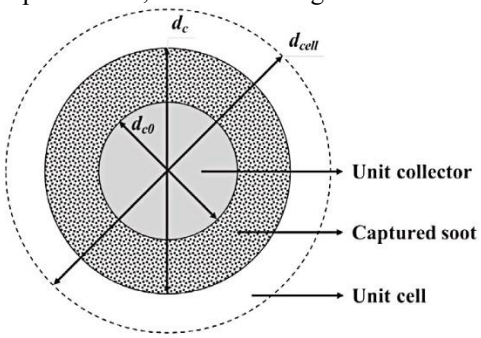

Fig. 2. Schematic of the unit collector.

A saturation coefficient of the filter wall was defined as:

$$\Phi = \frac{d_c^2 - d_{c0}^2}{(\Theta d_{cell})^2 - d_{c0}^2} \tag{1}$$

where d_{c0} represents the diameter of a clean unit collector, d_c refers to the diameter of the unit collector, d_{cell} refers to the diameter of the unit cell, and Θ is a control constant whose value is 0.92[10-12] in this study.

When Φ is 1, the unit cell is saturated and the deep-bed filtration phase ends.

2.1.2 Calculation model of DPF deep-bed filtration carbon load

Usually, the deep-bed filtration phase of DPF only lasts a few minutes [13]. However, the packing density of soot particles which deposited into the wall and on the wall have a large difference, the effect of the carbon loading of the deep-bed filtration phase on the pressure drop of the DPF cannot be ignored. Since there is no built-in the carbon loading model of the deep-bed filtration phase in AVL-Boost, the following calculation model is established to solve this problem.

The carbon loading in the deep-bed filtration phase can be expressed as:

$$SL_{deep} = \frac{m_{soot-wall-max}}{V_m} \tag{2}$$

where $m_{soot\text{-}wall\text{-}max}$ refers to the quality of soot trapped into the filter wall at the deep-bed filtration phase, V_m refers to the apparent volume of the DPF (without considering pores, porosity, etc.).

Related experiments and simulation studies show that most of the soot cannot penetrate the filter wall completely, but only deposits in a small part of the wall area below the surface of the DPF inlet channel [11, 13-17]. According to this, $m_{soot\text{-}wall\text{-}max}$ can be expressed as:

$$m_{soot-wall-max} = m_{soot-cell-max} \cdot N_{cell-load} \tag{3}$$

where $m_{soot\text{-}cell\text{-}max}$ refers to the maximum mass of soot that trapped in a single unit cell, $N_{cell\text{-}load}$ refers to the number of unit cells included in the wall load area.

$m_{soot\text{-}cell\text{-}max}$ can be expressed as:

$$m_{soot-cell-max} = \frac{4}{3}\pi \cdot [(\frac{\Theta d_{cell}}{2})^3 - (\frac{d_{c0}}{2})^3] \cdot \rho_{soot-wall} \tag{4}$$

where $\rho_{soot-wall}$ refers to the packing density of soot particles into the wall, the value is 345 kg/m^3 in this study [11,19].

For $N_{cell-load}$, it can be calculated as follows:

$$N_{cell-load} = \frac{S_f \cdot h_p}{\frac{4}{3}\pi \cdot (\frac{d_{cell}}{2})^3} \tag{5}$$

where S_f refers to the total filter cross-sectional area of the DPF, h_p refers to the soot penetration thickness of the wall load area, and unit is mil.

S_f can be calculated as:

$$S_f = \pi \cdot \left(\frac{D_m}{2}\right)^2 \cdot \frac{n}{2} \cdot 4 \cdot a \cdot L_m = 2n \cdot a \cdot V_m \tag{6}$$

where D_m is the filter diameter, L_m is the axial length of the filter, n is the cell density, and unit is CPSI, a refers to the side length of a square cell.

In addition, there is the following relationship between d_{cell} and d_{c0}:

$$d_{cell} = \frac{d_{c0}}{(1-\varepsilon_0)^{1/3}} \tag{7}$$

In the formula, ε_0 is the initial porosity of the DPF filter wall.

Based on the above relationship, SL_{deep} can be re-expressed as:

$$SL_{deep} = 2(\Theta^3 - 1 + \varepsilon_0) \cdot n \cdot a \cdot h_p \cdot \rho_{soot-wall} \tag{8}$$

For h_p, based on the data in the literature [11], this paper fits the functional relationship between h_p and d_{pore0}, the following expression was obtained:

$$h_p = -0.0005 \cdot d_{pore0}^2 + 0.051 \cdot d_{pore0} - 0.1798 \tag{9}$$

where d_{pore0} refers to the initial mean pore diameter of the filter, and unit is μm.

2.1.3 Calculation model of permeability of filter wall

For the wall-flow DPF, the pressure drop caused by the filter cake layer and the filter wall surface should be mainly considered, and calculated by Darcy's Law. Its expression is as follows:

$$\Delta p_w = \mu \frac{u h_w}{k_w} + \beta \rho u^2 h_w \tag{10}$$

where Δp_w refers to the pressure drop caused by fluid flowing through the porous medium, μ refers to the dynamic viscosity of the fluid, h_w refers to the thickness of the porous media wall, k_w refers to the permeability of the porous media wall, β refers to Forchheimer coefficient.

In AVL-Boost, there is no built-in calculation model for k_w, so the following compensation model is established in this paper [18]:

$$k_w = f(\varepsilon) \cdot d_c^2 \cdot SCF \tag{11}$$

Among them, the expression of $f(\varepsilon)$ is:

$$f(\varepsilon) = \frac{2}{9} \cdot \frac{2 - \frac{9}{5} \cdot (1-\varepsilon)^{\frac{1}{3}} - \varepsilon - \frac{1}{5} \cdot (1-\varepsilon)^2}{1-\varepsilon} \tag{12}$$

where ε refers to the porosity of the DPF filter wall

SCF is the Stokes-Cunningham coefficient reflecting the slip-flow effect, which can be calculated as follows:

$$SCF = 1 + Kn[1.257 + 0.4\, exp\left(-\frac{1.1}{Kn}\right)] \tag{13}$$

$$Kn = \frac{2\lambda}{d_{pore}} \tag{14}$$

$$\lambda = \frac{\mu}{\rho} \sqrt{\frac{\pi M r}{2 R_g T}} \tag{15}$$

where K_n refers to Knudsen number, λ refers to the gas mean free path, d_{pore} indicates the diameter of pores in the wall, Mr refers to the molecular weight, R_g refers to the universal gas constant, T refers to temperature.

2.2 Construction of DPF simulation model

The one-dimensional simulation model of DPF established in this paper, shown in Figure 3.

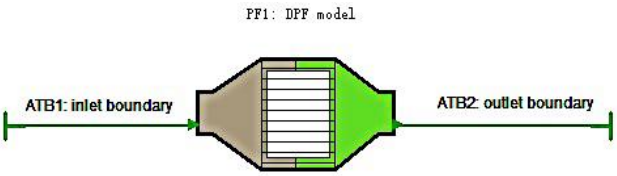

Fig. 3. One-dimensional simulation model of DPF.

In order to accurately calculate the DPF carbon loading in deep-bed filtration phase and the permeability of the DPF wall, the compensation mathematical model in 2.1 is embedded into the DPF simulation model. The primary technical parameters of the DPF are listed in Table 1.

Table 1. Technical parameters of the DPF.

Parameter	Value
Volume (L)	1-30
Length-to-diameter ratio (/)	0.7-2.0
Cell density (CPSI)	100-400
Wall thickness (mil)	8-20
Wall porosity (%)	25-65
Mean pore diameter (μm)	8-34
Thermal Conductivity (W/ (m.k))	0.85
Specific heat capacity (J/ (kg.K))	1046

3 Key performance parameters of DPF

3.1 filtration efficiency of particles in DPF

In this paper, the calculation of the filtration efficiency of PM and PN is based on the classical filtration theory in 2.1.1. This paper only considers the filtration efficiency of particles when DPF it is no-load. Once DPF enters the cake filtration phase, the filtration efficiency of particles will reach 100%, which has no reference point.

Two filtration mechanisms, namely the Brownian diffusion and the interception, were considered in this study. While other filtration mechanisms such as the inertial collision and the gravity deposition are ignored.

The filtration coefficient of the Brownian diffusion mechanism can be expressed as:

$$\eta_D = 3.5 \cdot g(\varepsilon)^{1/3} Pe^{-2/3} \tag{16}$$

Among them, $g(\varepsilon)$ is given by:

$$g(\varepsilon) = \frac{\varepsilon}{2 - \varepsilon - \frac{9}{5}(1-\varepsilon)^{1/3} - \frac{1}{5}(1-\varepsilon)^2} \tag{17}$$

where ε is equal to ε_0.

$$Pe = \frac{u d_c}{D_p} \tag{18}$$

where d_c is equal to d_{c0}.

$$d_{c0} = \frac{3}{2} \cdot \frac{1-\varepsilon_0}{\varepsilon_0} d_{pore0} \tag{19}$$

$$D_p = \frac{Tk_B SCF}{3\pi\mu d_{part}} \tag{20}$$

where k_B is the Boltzmann constant, d_{part} refers to the diameter of the particles to be trapped.

The filtration coefficient of the interception mechanism is given by:

$$\eta_R = 1.5 \cdot \frac{N_R^2}{1 + N_R^{\frac{3-2\varepsilon}{3\varepsilon}}} \cdot g(\varepsilon) \tag{21}$$

where ε is equal to ε_0.

$$N_R = \frac{d_{part}}{d_c} \tag{22}$$

where d_c is equal to d_{c0}.

Therefore, the combined filtration coefficient of these two mechanisms can be expressed as:

$$\eta_{DR} = \eta_D + \eta_R - \eta_D \eta_R \tag{23}$$

For particles of a certain size, the filtration efficiency is defined as:

$$E_{trap-single} = 1 - exp(-\frac{3 \cdot \eta_{DR}(1-\varepsilon)h}{2 \cdot \varepsilon d_c}) \tag{24}$$

where ε is equal to ε_0, d_c is equal to d_{c0}.

While the filtration efficiency of PM and PN can be expressed as:

$$FE - PM = \frac{\sum_k (N_{part,k} \cdot d_{part,k}^3 \cdot E_{trap-single,k})}{\sum_k (N_{part,k} \cdot d_{part,k}^3)} \tag{25}$$

$$FE - PN = \frac{\sum_k (N_{part,k} \cdot E_{trap-single,k})}{\sum_k N_{part,k}} \tag{26}$$

where N_{part} is the number of particles, k is the code of the particle size.

It can be seen that both FE-PM and FE-PN are less than 100% And the closer the value is to 100%, the higher the initial filtration efficiency of the DPF.

3.2 No-load pressure drop of DPF

The pressure drop caused by the wall-flow DPF is the highest in the diesel exhaust aftertreatment system. Therefore, the design concept of the DPF is to reduce the pressure drop on the premise of ensuring its filtration performance.

The pressure drop of DPF includes the local pressure loss at the entrance and exit of the DPF channel, the pressure loss along the way in the channel, and the pressure loss caused by

the filter cake layer and the filter wall surface (Eq. (10)). The calculation formulas for various pressure losses are as follows:

$$\Delta p_f = \lambda_f \frac{l}{d} \frac{\rho u^2}{2} \tag{27}$$

$$\Delta p_l = \zeta \frac{\rho u^2}{2} \tag{28}$$

where Δp_f is the pressure loss along the way, λ_f is the coefficient of pressure loss along the way, l is the channel length, and d is the channel hydraulic diameter; Δp_l is the local pressure loss, and ζ is the coefficient of the local pressure loss.

The local pressure loss and the pressure loss along the way are proportional to the square of the flow velocity u. However, the pressure losses caused by the filter cake layer and the filter wall surface are proportional to the power of u. It is difficult to construct an appropriate pressure loss coefficient for the DPF. Therefore, the absolute value of the pressure drop is used to calculate the no-load pressure drop (PD_{emp}) by this paper.

When calculating the value of PD_{emp}, this paper adopts the database-neural network model. First, based on the design of experiment (DoE) theory in AVL-Boost, a database including input parameters and corresponding value of PD_{emp} is constructed by simulation. Then, using the neural network learning method to train the database. Finally, a neural network model is established to directly calculate the no-load pressure drop under various conditions.

Input parameters and their value ranges required for DoE simulation are shown in Figure 4. 2000 sets of evenly distributed test points are generated in the input parameter space, and the value of PD_{emp} under each set of test points is calculated.

Design Variables : DoE - DPF1

Design Variables (Factors)

Design Variable	Variation Type	Lower Bound	Base	Upper Bound	Levels
V_M	Linear	1.0	15.0	30.0	2
LD	Linear	0.7	1.03	2.0	2
n	Linear	100.0	200.0	400.0	2
h	Linear	7.87	13.78	19.69	2
por0	Linear	0.25	0.55	0.65	2
dp0	Linear	8.0	10.0	34.0	2
T_in	Linear	200.0	300.0	600.0	2
GHSV	Linear	0.0	20000.0	80000.0	2

Fig. 4. Input parameters and their value ranges in DoE simulation of PD_{emp},
(*V_M*: Apparent volume of the DPF; *LD*: Length-to- Diameter ratio; *n*: Cell density; *h*: wall thickness; *por0*: Initial porosity of the filter wall; *dp0*: Initial mean pore diameter of the filter; *T_in:* Inlet gas temperature (℃); *GHSV*: Space velocity (h^{-1}))

When the simulation is completed, the three-layer BP neural network in Matlab software is used to train the result. The proportion of the training set is 90%, the ratios of the verification set and the test set are both 5%. The training results are shown in Figure 5.

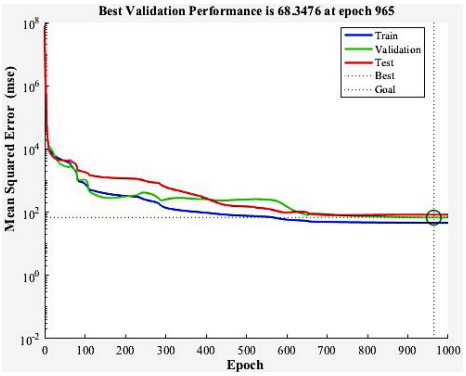

Fig. 5. Neural network training results of PD_{emp}.

3.3 DPF pressure drop under the maximum carbon load

The DPF pressure drop under the maximum carbon load (PD_{max}) determines the average pressure drop during the life cycle of the DPF. Therefore, PD_{max} is regarded as one of the key performance parameters of the DPF.

The calculation of PD_{max} is similar to PD_{emp}. The input parameters and value ranges of the DoE simulation of the DPF pressure drop under the maximum carbon load are shown in Figure 6. 3000 sets of evenly distributed test points are generated in the input parameter space, and the value of PD_{max} under each set of test points is calculated by AVL-Boost.

Design Variables : DoE - DPF1

Design Variables (Factors)

Design Variable	Variation Type	Lower Bound	Base	Upper Bound	Levels
V_M	Linear	1.0	15.0	30.0	2
LD	Linear	0.7	1.03	2.0	2
n	Linear	100.0	200.0	400.0	2
h	Linear	7.87	13.78	19.69	2
por0	Linear	0.25	0.55	0.65	2
dp0	Linear	8.0	10.0	34.0	2
T_in	Linear	200.0	300.0	600.0	2
GHSV	Linear	0.0	20000.0	80000.0	2
sootmass_initial	Linear	0.0	5.0	10.0	2

Fig. 6. Input parameters and their value ranges in DoE simulation of $PD_{max.}$
(*sootmass_initial*: Carbon loading in the DPF, g/L)

The training algorithm of the neural network is similar to PD_{emp}, and the training results are shown in Figure 7.

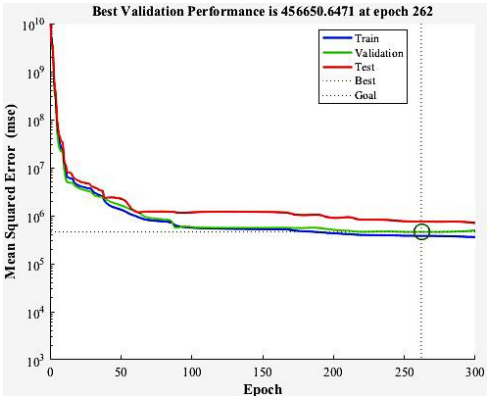

Fig. 7. Neural network training results of $PD_{max.}$

4 Results and discussion

4.1 Influence of cell density and wall thickness on DPF filtration efficiency

Fig 8 and Fig 9 respectively show the effects of different cell densities and wall thicknesses on the filtration efficiency of PM and PN when other conditions are constant. It can be seen that as the cell density and wall thickness increase, the filtration efficiencies of PM and PN increase. When the cell density increases, the surface area of the DPF channel increases and the gas flow rate in the wall decreases, which causes the filtration coefficient of the Brownian diffusion (η_D) to increase. When the wall thickness increases, the surface area of the DPF channel decreases, resulting in a decrease of η_D. In addition, according to equation (24), the increase of wall thickness will directly increase the filtration efficiency of a single particle ($E_{trap-single}$). Of the above two influences, the latter has a greater weight, so an increase in the wall thickness of the substrate can improve the filtration efficiency of the DPF.

Therefore, the increase of DPF cell density and wall thickness will increase the filtration efficiencies of PM and PN.

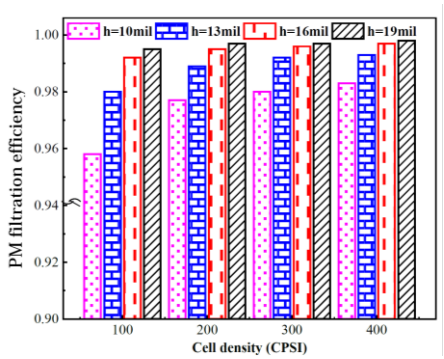

Fig. 8. Influence of the DPF cell density and wall thickness on the PM filtration efficiency under certain conditions.
(Apparent volume of the filter: 10L; Length-to-diameter ratio: 1.03; Initial porosity of the filter wall: 0.55; Initial mean pore diameter of the filter: 10μm; The inlet gas temperature: 250℃; Gas volume flow: 250000L/h)

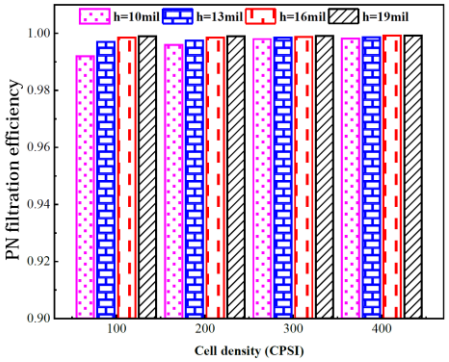

Fig. 9. Influence of the DPF cell density and wall thickness on the PN filtration efficiency under certain conditions.
(Apparent volume of the filter: 10L; Length-to-diameter ratio: 1.03; Initial porosity of the filter wall: 0.55; Initial mean pore diameter of the filter: 10μm; The inlet gas temperature: 250℃; Gas volume flow: 250000L/h)

4.2 Influence of cell density and wall thickness on DPF no-load pressure drop

Under the certain conditions, the influence of the substrate cell density and wall thickness on the no-load pressure drop is shown in Figure 10. The larger of the cell density and the wall thickness, the smaller of the substrate opening area and the cell hydraulic diameter, so that the local pressure loss at the entrance and exit of the filter is significantly increased. Therefore, the no-load pressure drop of the DPF is higher. In addition, the increase of the wall thickness will increase the pressure loss when the gas flows through the wall. So, the larger the wall thickness, the greater the slope of the no-load pressure drop curve.

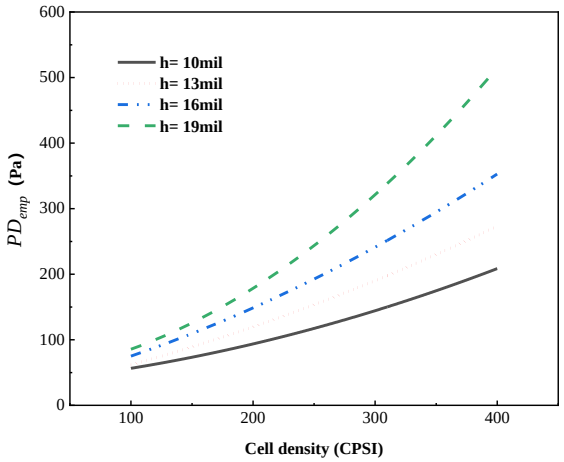

Fig. 10. Influence of the substrate cell density and wall thickness on the DPF no-load pressure drop under certain conditions
(Apparent volume of the filter: 10L; Length-to- diameter ratio: 1.03; Initial porosity of the filter wall: 0.55; Initial mean pore diameter of the filter: 10μm; The inlet gas temperature: 250℃; Gas volume flow: 100000L/h)

4.3 Influence of cell density and wall thickness on DPF pressure drop under the maximum carbon load

Figure 11 shows the effect of the substrate cell density and wall thickness on the DPF pressure drop when the maximum carbon load is 7g/L and other conditions are constant. It can be seen that the increase of the cell density can significantly reduce the DPF pressure drop under the maximum carbon load. According to formula (8), the carbon loading of DPF deep-bed filtration phase will increase with the increase of cell density, as shown in Figure 12. Under the same total carbon load, With the increase of the substrate cell density, more soot particles will be deposited in the wall instead of the filter cake layer. According to relevant literatures, the permeability of the filter wall is 1 to 2 orders of magnitude higher than that of the filter cake layer under full carbon load. Although the increase of the cell density will cause the increase of the local pressure loss of the DPF channel, the influence weight of the former mechanism is greater, so that the DPF pressure drop under the carbon load is reduced.

When the wall thickness increases, the local pressure loss at the entrance/exit of the channel and the pressure loss caused by the gas flowing through the wall will increase. And the carbon load in the deep-bed filtration phase will decrease, as shown in Figure 12. Therefore, the DPF pressure drop under the carbon load will increase significantly.

In conclusion, under the carbon load, the increase of the substrate cell density will reduce the DPF pressure drop, while the increase of the wall thickness will increase the DPF pressure drop.

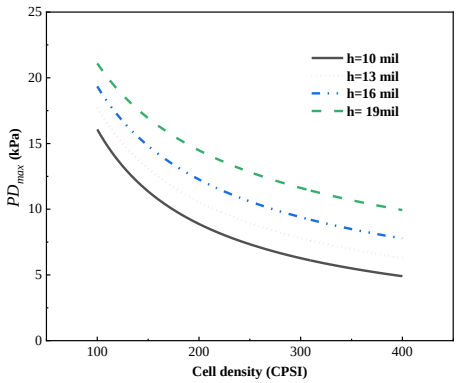

Fig. 11. Influence of the substrate cell density and wall thickness on the DPF load pressure drop under certain conditions.
(Apparent volume of the filter: 10L; Length-to- diameter ratio: 1.03; Initial porosity of the filter wall: 0.55; Initial mean pore diameter of the filter: 10μm; The inlet gas temperature: 250℃; Gas volume flow: 100000L/h; Carbon load: 7g/L)

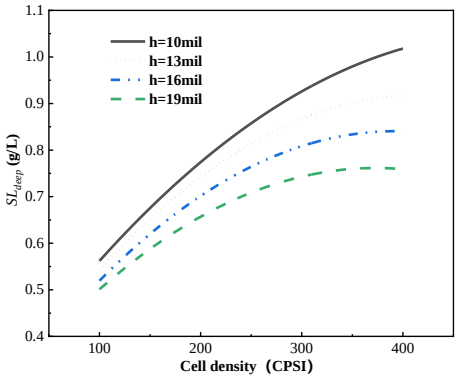

Fig. 12. Influence of the substrate cell density and wall thickness on the DPF carbon load in the deep-bed filtration phase under certain conditions.
(Initial porosity of the filter wall: 0.55; Initial mean pore diameter of the filter: 10μm)

5 Conclusions

1) In this paper, a mathematical model of the DPF carbon load in the deep-bed filtration phase and the permeability of the filter wall was established and embedded into the DPF simulation model.

2) With the increase of the substrate cell density, the filtration efficiencies of PM and PN increased, the DPF pressure drop under the maximum carbon load reduced, but the DPF no-load pressure drop increased.

3) With the decrease of the filter wall thickness, the DPF no-load pressure drop decreased, the DPF pressure drop under the maximum carbon load reduced, but the filtration efficiencies of PM and PN decreased.

4) The larger the cell density and the smaller the wall thickness, the lower the pressure drop of the DPF. Also considering the filtration efficiencies of PM and PN, the most suitable combination scheme is the cell density of 200-300 CPSI and the wall thickness of 11-16 mil.

This work was supported by the National Key R&D Program of China [2017YFC0211202]; and the Prospective study funding of Nanchang Automotive Innovation Institute [QZKT2020-07]. The authors would like to thank the editors and anonymous reviewers for their suggestions to improve the paper.

References

1. Liu JH, Sun P, Huang H, et al. Experimental investigation on performance, combustion and emission characteristics of a common-rail diesel engine fueled with polyoxymethylene dimethyl ethers-diesel blends[J]. Applied Energy, 2017, 202: 527-536.
2. Jain A, Singh AP, Agarwal AK. Effect of split fuel injection and EGR on NOx and PM emission reduction in a low temperature combustion (LTC) mode diesel engine[J]. Energy, 2017, 122: 249-264.
3. Fiebig M, Wiartalla A, Holderbaum B, et al. Particulate emissions from diesel engines: correlation between engine technology and emissions[J]. Journal of Occupational Medicine and Toxicology, 2014, 9(1): 6.
4. Zhang B, E JQ, Gong JK, et al. Influence of structural and operating factors on performance degradation of the diesel particulate filter based on composite regeneration[J]. Applied Thermal Engineering, 2017, 121: 838-852.
5. Pontikakis G, Stamatelos A. Stamatelos, Three-dimensional catalytic regeneration modeling of SiC diesel particulate filters[J]. Journal of Engineering for Gas Turbines and Power-Transactions of the Asme, 2006, 128(2): 421-433.
6. Williams AM, Garner CP, Binner JGP. Analysis and optimization of gel-cast ceramic foam diesel particulate filter performance[J]. Proceedings of the Institution of Mechanical Engineers Part D-Journal of Automobile Engineering, 2008, 222(D11): 2235-2247.
7. Cordiner S, mecocci F, Mulone V, Nobile M. Model Based Design Procedure of After Treatment Systems for Non-Road Diesel Engines[C]. SAE International, 2011.
8. Deng YW, Zheng WP, E JQ, et al. Influence of geometric characteristics of a diesel particulate filter on its behavior in equilibrium state[J]. Applied Thermal Engineering, 2017, 123: 61-73.
9. Lupse J, Campolo M, Soldati A. Modelling soot deposition and monolith regeneration for optimal design of automotive DPFs[J]. Chemical Engineering Science, 2016, 151: 36-50.
10. Tan PQ, Cao CY, Hu ZY, et al. Modeling of soot fragmentation that proceeds in a catalyzed diesel particulate filter of a diesel engine[J]. Chemical Engineering Journal, 2019, 375.
11. Serrano JR, Arnau FJ, Piqueras P, et al. Packed bed of spherical particles approach for pressure drop prediction in wall-flow DPFs (diesel particulate filters) under soot loading conditions[J]. Energy, 2013, 58: 644-654.
12. Serrano JR, Climent H, Piqueras P, et al. Filtration modelling in wall-flow particulate filters of low soot penetration thickness[J]. Energy, 2016, 112: 883-898.
13. Bensaid S, Marchisio DL, Fino D, et al. Modelling of diesel particulate filtration in wall-flow traps[J]. Chemical Engineering Journal, 2009, 154(1-3): 211-218.
14. Yapaulo RA, Wirojsakunchai E, Orita T, et al. Impact of filtration velocities and particulate matter characteristics on diesel particulate filter wall loading[J]. International Journal of Engine Research, 2009, 10(5): 287-304.

15. Fino D, Russo N, Millo F, et al. New Tool for Experimental Analysis of Diesel Particulate Filter Loading[J]. Topics in Catalysis, 2009, 52(13-20): 2083-2087.
16. Yamamoto K, Satake S, Yamashita H, et al., Lattice Boltzmann simulation on porous structure and soot accumulation[J]. Mathematics and Computers in Simulation, 2006, 72(2-6): 257-263.
17. Yamamoto K, Oohori S, Yamashita H, et al. Simulation on soot deposition and combustion in diesel particulate filter[J]. Proceedings of the Combustion Institute, 2009, 32: 1965-1972.
18. Konstandopoulos A. Flow resistance descriptors for diesel particulate filters: definitions, measurements and testing[C]. SAE Technical Paper, 2003, 2003-01-0846.
19. Konstandopoulos A.G, Kostoglou M, Skaperdas E, et al. Fundamental studies of diesel particulate filters: transient loading, regeneration and aging[C]. SAE Technical Paper, 2000, 2000-01-1016.